Formation of Organic Crystalline Nanopillar Arrays and Their Application to Organic Photovoltaic Cells

Masaya Hirade,[†,‡] Hajime Nakanotani,[†,‡] Masayuki Yahiro,[†,‡,§] and Chihaya Adachi*[,†,‡,§]

Center for Organic Photonics and Electronics Research (OPERA) and Center for Future Chemistry, Kyushu University, 744 Motooka, Nishi, Fukuoka, 819-0395, Japan, Bio Electromechanical Autonomous Nano-Systems (BEANS) Laboratory, Life Beans Center Kyushu, 744 Motooka, Nishi, Fukuoka, 819-0395, Japan, Institute of Systems, Information Technologies and Nanotechnologies 2-1-22, Momochihama, Sawara, Fukuoka 814-0001, Japan

ABSTRACT To enhance the performance of organic photovoltaic (OPV) cells, preparation of organic nanometer-sized pillar arrays is fascinating because a significantly large area of a donor/acceptor heterointerface having continuous conduction path to both anode and cathode electrodes can be realized. In this study, we grew cupper phthalocyanine (CuPc) crystalline nanopillar arrays by conventional thermal gradient sublimation technique using a few-nanometer-sized trigger seeds composed of a CuPc and 3,4,9,10-perylene-tetracarboxylic-dianhydride (PTCDA) stacked layer. We optimized the pillar density by tuning crystal growth condition in order to apply it to OPV cells.

KEYWORDS: nanopillar arrays • molecular orientation control • PTCDA • CuPc • organic photovoltaic cell

INTRODUCTION

Recently, the power conversion efficiency (η_{PCE}) of organic photovoltaic (OPV) cells has been increased dramatically (1–6). However, their η_{PCE} values are still lower than those of inorganic cells. To enhance the η_{PCE} of OPV cells, morphological control of organic donor/acceptor interfaces achieved by introducing nanostructures is thought to be crucial because the exciton diffusion length of organic materials is quite short, typically less than 10 nm (7). For example, it has been well-established that bulk heterojunction OPV cells containing codeposited low molecular weight materials (2, 3) or phase-separated polymer materials (4, 5) show higher η_{PCE} than OPV cells with conventional simple planar heterojunction structures. This is because the more complex structures provide a donor/acceptor heterointerface of larger area. However, the uncontrolled random distribution of donor and acceptor units would result in the formation of locally discontinuous carrier conduction pathways, leading to the formation of carrier trapping sites and a low carrier collection efficiency. To maximize carrier separation and collection efficiencies, well-controlled donor/acceptor heterointerfaces composed of artificial nanostructures are required. In particular, 20–30 nm sized pillar arrays are ideal for this concept (8–11) because these structures provide high-efficiency exciton dissociation with efficient carrier transport to both the cathode and anode.

Nanopillar arrays have been formed by both top-down and bottom-up approaches. Nanoimprinting has been widely used as a top-down process (9, 10). However, because the application of this technique to produce organic thin films using 100 nm sized fine molds is problematic, particularly the delamination process, bottom-up approaches are more realistic for practical device fabrication to obtain a uniform large area. In this paper, we report the formation of crystalline nanopillar arrays using a completely dry fabrication process and the application of these arrays in OPV cells.

EXPERIMENTAL METHODS

For nanopillar formation, a simple seeding technique was used. Nanopillars were grown by conventional thermal gradient sublimation (12) on a layer of tiny seed crystals with a size of several tens of nm. Here, copper phthalocyanine (CuPc) was used as an electron donating material for pillar formation. Because CuPc single crystals usually show needlelike structures, nanopillar arrays were anticipated to form on a seed layer. To grow CuPc nanopillar arrays on a substrate, we first prepared a seed layer composed of 3,4,9,10-perylene-tetracarboxylic-dianhydride (PTCDA) (3 nm)/CuPc (3 nm), which was formed by conventional vacuum deposition. When the seed layer is composed of CuPc alone, the growth direction of CuPc crystals was along the plane of the substrate (Figure 1a) because the CuPc seeds had an edge-on orientation on the substrate (13). In contrast, when a PTCDA/CuPc stacked layer was formed, the first layer of deposited PTCDA molecules showed a face-on orientation on the substrate and the successive CuPc layer showed a horizontal orientation (13–17), resulting in the face-on orientation of the CuPc layer during growth of the CuPc pillars. Thus, the CuPc molecules showed a face-on orientation in the pillars (Figure 1a), which is the ideal structure in terms of carrier transport.

* Corresponding author. Tel.: +81-92-802-6923. Fax: +81-92-802-6921. E-mail: adachi@cstf.kyushu-u.ac.jp.
† Kyushu University.

‡ Life Beans Center Kyushu.

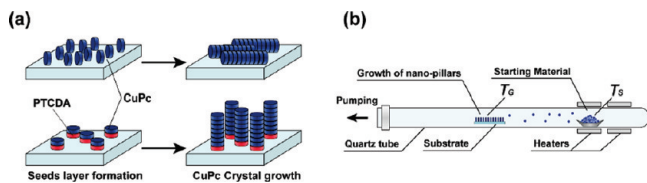§ Institute of Systems, Information Technologies and Nanotechnologies.

FIGURE 1. Schematic illustration of (a) CuPc pillar growth characteristics with each seed layer and (b) sublimation system for crystalline pillar formation.
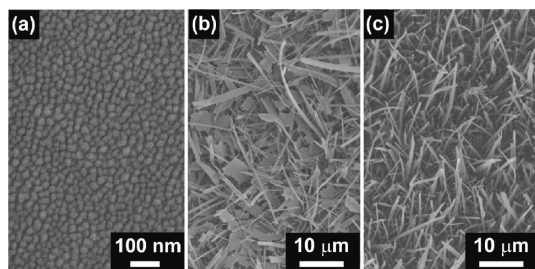

FIGURE 2. SEM images of (a) the PTCDA/CuPc seed layer and CuPc crystals (b) on a CuPc seed layer and (c) on a PTCDA/CuPc seed layer at source temperature of T_S = 370 °C and a growth temperature of T_G = 215 °C.

The PTCDA, CuPc, and bathocuproine (BCP) used in this study were purchased from Tokyo Chemical Industry and were purified twice by conventional sublimation. For device fabrication, indium tin oxide (ITO)-coated glass substrates were first washed with neutral detergent and organic solvent and cleaned by UV/O₃ treatment. Then, 3 nm thick PTCDA and 3 nm thick CuPc stacked seed layers were formed by vacuum deposition under a vacuum of <1 × 10⁻³ Pa on the ITO substrate with a deposition rate of ∼0.01 nm/s. The substrate was transferred into a vacuum sublimation chamber with unavoidable exposure to the air. CuPc pillar arrays were grown on the substrate in a quartz tube under vacuum (∼1 × 10⁻² Pa) as shown in Figure 1b. The source temperature (T_S) and growth temperature (T_G) were kept at 355−380 °C and 85−215 °C, respectively. After crystal growth, the substrate was transferred into a glovebox with re-exposure to the air. An acceptor layer of 6,6-phenyl-C₆₁-butyric acid methyl ester (PCBM) was applied by spin-coating. PCBM was dissolved in chlorobenzene (30 mg/mL) and spun onto the CuPc layer (2500 rpm, 60 s). The substrate was then baked at 120 °C for 3 min. The substrate was transferred into a vacuum chamber and a BCP layer with a thickness of 10 nm was deposited on the active layer to act as a hole-blocking layer. Finally, an Ag top electrode (50 nm) was deposited onto the organic layer through a shadow mask with circular openings of 1 mm diameter. η_{PCE} and current density−voltage (J−V) characteristics were measured under AM 1.5 G illumination at 100 mW/cm², which was supplied by a solar simulator (OTENTO-SUN II, Bunko-Keiki Co.), using a semiconductor parameter analyzer (4156C/41501B, Agilent Co.). All measurements were conducted under vacuum. The molecular orientation of CuPc was measured by X-ray diffraction (XRD, Ultima IV, Rigaku Co., Cu−Kα, λ = 1.54 Å), and the CuPc nanopillar arrays were characterized by field-emission scanning electron microscopy (FE-SEM, JSM-6701F, JEOL Co.).

RESULTS AND DISCUSSION

Figure 2a shows the PTCDA (3 nm)/CuPc (3 nm) stacked layer on a SiO₂ substrate, which exhibit small island structures. CuPc pillar structures were grown using this seed layer. Although flake-like CuPc crystals possessing a parallel orientation to the substrate were obtained on a CuPc seed
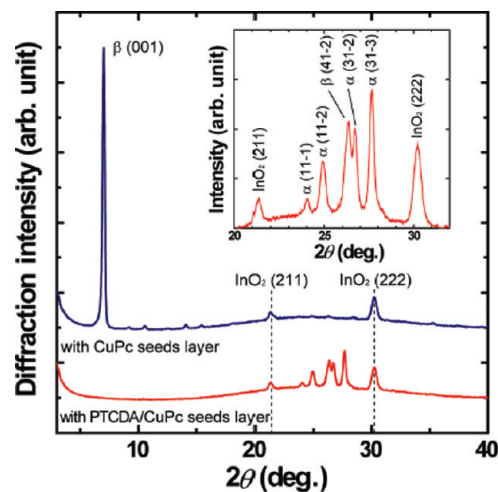

FIGURE 3. XRD patterns of CuPc crystals on CuPc and PTCDA/CuPc seed layers. Inset: Schematic view of the growth direction of CuPc crystals. Inset: Close-up XRD pattern of CuPc crystals on PTCDA/CuPc seed layer and Miller indices of peaks.

layer (Figure 2b), ideal wirelike CuPc pillar arrays that grew perpendicular to the substrate were obtained using the PTCDA/CuPc seed layer (Figure 2c).

The XRD patterns of the two obtained structures provided further confirmation of these differences. Figure 3 shows the XRD patterns of the CuPc nanopillar arrays grown on CuPc and PTCDA/CuPc seed layers. With a CuPc seed layer, a diffraction peak at 2θ = 7.02° was obtained and its d spacing was d = 0.704 nm, which corresponds to the β(001) plane (18), indicating that the b-axis of the CuPc molecules was parallel to the substrate. On the other hand, with a PTCDA/CuPc seed layer, the diffraction peak at 2θ = 7.02° disappeared and other diffraction peaks at 24.03, 24.92, 26.35, 26.70, and 27.67° were obtained. Their d specings were d = 0.370, 0.357, 0.338, 0.333, and 0.322 nm, respectively, and they corresponded to the α(11−1), α(11−2), β(41−2), α(31−2), and α(31−3) planes, respectively (18). This indicates that the b-axis of the CuPc molecules was perpendicular to the substrate. Thus, the growth of CuPc nanopillar arrays was successfully achieved by the use of a PTCDA/CuPc seed layer.

Because the obtained CuPc nanopillars were rather long, the crystal growth conditions were optimized for application of the nanopillar arrays in OPV devices. SEM images of the nanopillar arrays obtained under controlled growth conditions are shown in Figure 4a−d. In the conditions used to produce the film shown in (a), the growth temperature was kept at T_S = 355 °C and T_G = 150 °C and heating was maintained for a short time of a few minutes. Although the length of each pillar was well controlled between several tens of nanometers and several hundred nanometers, the distance between the adjacent pillars was around 100 nm, which is rather wide compared with the exciton diffusion length of a PCBM layer (>5 nm) (19). Here, we supposed that aggregation of the seeds occurred during heat annealing. Thus, pillar arrays were grown at the lower temperature of T_G = 85 °C. Figure 4b shows an SEM image of the CuPc nanopillar arrays grown at T_S = 380 °C and T_G = 85 °C.
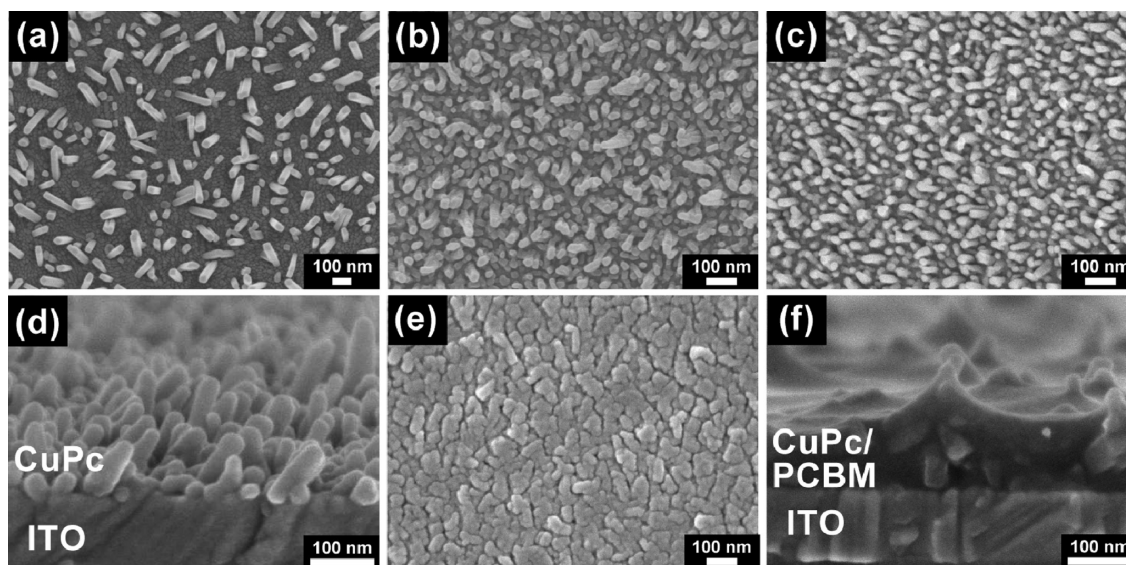
FIGURE 4. SEM images of CuPc crystalline pillar structures grown on an ITO substrate. (a) $T_S = 350$ °C and $T_G = 150$ °C, (b) $T_S = 380$ °C and $T_G = 85$ °C, (c) $T_S = 380$ °C and $T_G = 85$ °C on a MoO$_X$/PTCDA/CuPc layer, (d) cross-sectional view of c, (e) $T_S = 380$ °C and $T_G = 85$ °C on a MoO$_X$/CuPc layer, and (f) OPV active layer fabricated by deposition of PCBM on the array shown in d.
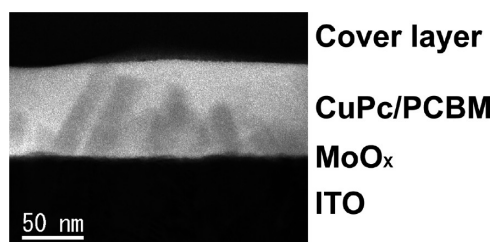

FIGURE 5. TEM images of active layer.

FIGURE 6. J–V characteristics of OPV cells using MoO$_X$/PTCDA/CuPc (red) and MoO$_X$/CuPc (black) seed layers under illumination (open circles) and in the dark (filled circles). Inset: Cell performance of the devices.

Here, to prevent leakage current, a 3 nm thick MoO$_X$ buffer layer was deposited on the ITO substrate, with the aim of producing an OPV device (20). Thus, the PTCDA/CuPc seed layer was deposited on an MoO$_X$ buffer layer and the CuPc pillar structures were grown on it (Figure 4c). The cross-sectional SEM image of these CuPc crystalline nanopillar arrays (Figure 4d) shows that high-density CuPc pillar arrays were obtained with pillars 30 nm in diameter and $10-100$ nm in length. In the case of the MoO$_X$/CuPc layer as a seed layer, CuPc nanopillar arrays could not be obtained (Figure 4e) because CuPc molecules in the seed layer showed edge-on orientation.

To confirm the existence of voids at the CuPc/PCBM interface, we obatined the TEM image. Figure 5 shows the TEM image of an ITO/MoO$_X$/nanopillar arrays/PCBM layer. From this image, CuPc nanopillar arrays were clearly observed and there were no voids at the interface. Thus, we conclude that the infiltration of PCBM into the CuPc pillars occurred sufficiently using our spin-coating method.

Finally, the nanopillar arrays were applied to OPV cells. Figure 6 shows the J–V characteristics of OPV cells containing the CuPc nanopillar arrays grown on CuPc and PTCDA/CuPc seed layer under illumination and in the dark. In the case of a CuPc seed layer, the cell exhibited the short circuit current of $J_{SC} = -1.54$ mA/cm^2, the open circuit voltage of $V_{OC} = 0.60$ V, the fill factor of FF $= 0.44$, and $\eta_{PCE} = 0.40\%$. In the case of a PTCDA/CuPc seed layer, the cell gave $J_{SC} =$
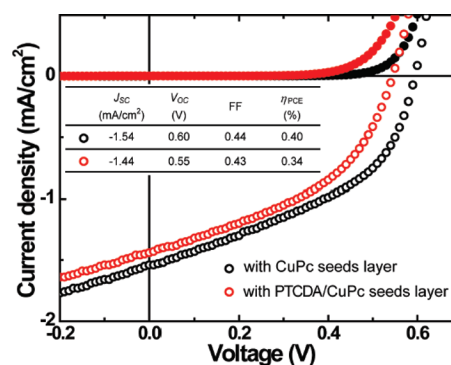
-1.44 mA/cm^2, $V_{OC} = 0.55$ V, FF $= 0.43$, and $\eta_{PCE} = 0.34\%$. The devices showed almost the same J_{SC} and η_{PCE}, even though the device containing a PTCDA/CuPc seed layer possessed a donor/acceptor heterointerface with a larger area. While the detailed mechanism of operation is unclear, we suppose that the adsorption of moisture and oxygen onto the donor/acceptor heterointerface during the device fabrication process significantly degraded the device performance. To obtain better device performance, we require control over the pillar length and a fabrication process that does not expose the device to air. Another reason for the similar J_{SC} and η_{PCE} could be related to the electronic characteristics of the PTCDA template layer, which would act as a carrier trapping site between the ITO and CuPc layers due to its deep HOMO level ($\sim$6.8 eV) (21). Furthermore, the active layer has a rather rough surface due to the presence of nanopillars of different length, which would lead to deterioration of OPV performance (Figure 4f). Additionally, we suppose exciton dissociation efficiency at the donor/acceptor interface is different between the reference and nanopillar cells. Since the direction of built-in electrical field (E) at the interface is different in these devices, i.e., lateral

 Hirade et al.

direction of E in the pillar device and vertical direction of E in the reference device, it will also influence the device performance.

CONCLUSION

In summary, CuPc crystalline nanopillar arrays were formed using a PTCDA/CuPc seed layer. The density and length of the nanopillar arrays were well-controlled by tuning the crystal growth temperature, and the structures were applied in OPV cells. Although a significant improvement in device performance was not obtained, better control over the pillar length along with an improved fabrication process will allow efficient OPV cells to be realized using this design.

REFERENCES AND NOTES

(1) Tang, C. W. *Appl. Phys. Lett.* **1986**, *48*, 183.
(2) Hiramoto, M.; Fujiwara, H.; Yokoyama, M. *Appl. Phys. Lett.* **1991**, *58*, 1062.
(3) Xue, J.; Rand, B. P.; Uchida, S.; Forrest, S. R. *Adv. Mater.* **2005**, *17*, 66.
(4) Reyes, M. R.; Kim, K.; Carrol, D. L. *Appl. Phys. Lett.* **2005**, *87*, 083056.
(5) Liang, Y.; Xu, Z.; Xia, J.; Tsai, S. T.; Wu, Y.; Li, G.; Ray, C.; Yu, L. *Adv. Mater.* **2010**, *22*, E135.
(6) Yang, F.; Sun, K.; Forrest, S. R. *Adv. Mater.* **2007**, *19*, 4166.
(7) Peumans, P.; Yakimov, A.; Forrest, S. R. *J. Appl. Phys.* **2003**, *93*, 3693.
(8) Yang, F.; Shtein, M.; Forrest, S. R. *Nat. Mater.* **2005**, *4*, 37.
(9) Aryal, M.; Buyukserin, F.; Mielczarec, K.; Zhao, X. M.; Gao, J.; Zakhidov, A.; Hu, W. *J. Vac. Sci. Technol., B* **2008**, *26*, 2562.
(10) Kim, J. S.; Park, Y.; Lee, D. Y.; Lee, J. H.; Park, J. H.; Kim, J. K.; Cho, K. *Adv. Funct. Mater.* **2010**, *20*, 540.
(11) Zheng, Y.; Bekele, R.; Ouyang, J.; Xue, J. *Org. Electron.* **2009**, *10*, 1621.
(12) Forrest, S. R. *Chem. Rev.* **1997**, *97*, 1793.
(13) Forrest, S. R.; Burrows, P. E.; Haskal, E. I.; So, F. F. *Phys. Rev. B* **1994**, *49*, 11309.
(14) Chen, W.; Huang, H.; Chen, S.; Gao, X. Y.; Wee, A. T. S. *J. Phys. Chem. C* **2008**, *112*, 5036.
(15) Sullivan, P.; Joenes, T. S.; Ferguson, A. J.; Heutz, S. *Appl. Phys. Lett.* **2007**, *91*, 233114.
(16) Heutz, S.; Coots, R.; Jones, T. S. *Appl. Phys. Lett.* **2000**, *77*, 3938.
(17) Sakurai, T.; Fukasawa, R.; Saito, K.; Akimoto, K. *Org. Electron.* **2007**, *8*, 702.
(18) Debe, M. K.; Kan, K. K. *Thin Solid Films* **1990**, *186*, 289.
(19) Cook, S.; Furube, A.; Han, L. *Chem. Phys. Lett.* **2009**, *478*, 33.
(20) Li, N.; Forrest, S. R. *Appl. Phys. Lett.* **2009**, *95*, 123309.
(21) Maruyama, T.; Hirasawa, A.; Shindow, T.; Akimoto, K.; Kato, H.; Kakizaki, A. *J. Lumin.* **2000**, *87*, 782.

AM100915S

ARTICLE